3D printing PLGA: a quantitative examination of the effects of polymer composition and printing parameters on print resolution

3D Printing PLGA: A Quantitative Examination of the Effects of Polymer Composition and Printing Parameters on Print Resolution

Ting Guo[1], Timothy R. Holzberg[1], Casey G. Lim[1], Feng Gao[2], Ankit Gargava[3], Jordan E. Trachtenberg[4], Antonios G. Mikos[4], and John P. Fisher[1]

[1]The Fischell Department of Bioengineering, University of Maryland, College Park, MD
[2]Department of Biological Statistics & Computational Biology, Cornell University, NY
[3]Department of Chemical and Biomolecular Engineering, University of Maryland, College Park, MD
[4]Department of Bioengineering, Rice University, Houston, TX

Short Title: 3D Printing PLGA

Key Words: poly(lactic-co-glycolic acid), scaffold, biomaterial, 3D printing, statistical analysis

Submitted To: Biofabrication

***Corresponding Author:** John P. Fisher, Ph.D.
Fischell Family Distinguished Professor and Department Chair
Fischell Department of Bioengineering
University of Maryland
2330D Jeong H. Kim Engineering Building
College Park, Maryland 20742
Phone: 301 314 2188
Email: jpfisher@umd.edu
Web: www.teblumd.net

Abstract

In the past few decades, 3D printing has played a significant role in fabricating scaffolds with consistent, complex structure that meets patient-specific needs in future clinical applications. Although many studies have contributed to this emerging field of additive manufacturing, which includes material development and computer-aided scaffold design, current quantitative analyses do not correlate material properties, printing parameters, and printing outcomes to a great extent. A model that correlates these properties has tremendous potential to standardize 3D printing for tissue engineering and biomaterial science. In this study, we printed poly(lactic-*co*-glycolic acid) (PLGA) utilizing a direct melt extrusion technique without additional ingredients. We investigated PLGA with various lactic acid:glycolic acid (LA:GA) molecular weight ratios and end caps to demonstrate the dependence of the extrusion process on the polymer composition. Micro-computed tomography (microCT) was then used to evaluate printed scaffolds containing different LA:GA ratios, composed of different fiber patterns, and processed under different printing conditions. We built a statistical model to reveal the correlation and predominant factors that determine printing precision. Our model showed a strong linear relationship between the actual and predicted precision under different combinations of printing conditions and material compositions. This quantitative examination establishes a significant foreground to 3D print biomaterials following a systematic fabrication procedure. Additionally, our proposed statistical models can be applied to couple specific biomaterials and 3D printing applications for patient implants with particular requirements.

Introduction

Tissue engineering has successfully enabled the development of biological substitutes that restore, maintain, or improve tissue function for therapeutic purposes [1]. However, the complexity of the native tissue environment creates challenges to successfully promote tissue regeneration. In order to maintain desired cell phenotypes and guide the cells to form functional tissue structures, 3D scaffolds have been applied and proven to have positive impact in the field of tissue engineering [2, 3]. Numerous studies have demonstrated the importance and success of 3D scaffolds to maintain appropriate cell morphology and promote differentiation [4, 5].

While cell therapy for tissue engineering needs further consideration and regulation on source selection, and cell phenotype stability, which slows the development of effective treatment, acellular approaches have been explored in regenerative medicine [6]. In the field of engineering scaffolds utilizing 3D printing technology, the acellular scaffolds approaches have much more choices in terms of materials and processing conditions compared to the cell laden approaches. For clinical applications, the acellular scaffolds can avoid the potential immune response from allogeneic cells and extra maintenance of the cells on the shelf.

One of the challenges that the conventional molded acellular scaffold has is the difficulty to capture the tissue structure. Recently, the advancement of 3D printing technologies provides new avenues for the fabrication of scaffolds with detailed structure to recapitulate the desired organization of native tissue or organ. In particular, for the fabrication of scaffolds to treat osteochondral defects, extrusion-based printing is one of the most popular fabrication methods due to its favored layer-by layer features with multiple solidification ways such as pH, temperature change or photocrosslinking [7, 8], and its relatively fast fabrication process compared to stereolithography. During manufacturing, complex 3D structure can be virtually sectioned to layers by associated software first, and then created layer by layer, as materials are deposited on the printing platform. With this technique, another advantage is the high quality of the interconnected pores as defined in the computer-aided design (CAD) model [9, 10]. During the scaffolds building, the fiber orientation can be controlled precisely with a resolution of around 100 μm. The mechanical properties of the printed scaffold can be greatly influenced by the fiber orientations [11].

While many different materials have been assessed for 3D printing, due to the lack of systematic research on the printing procedures, the reported fabrication methods are specific and case-dependent. Our present study utilizes an advanced evaluation process incorporating microCT scanning and computational statistic modeling to investigate the correlation between printing parameters and the resulting printing resolution.

Previous work on printing poly(propylene fumarate) has offered a conceptual method to evaluate the effects of material composition and printing parameters on scaffold architecture [12]. Our current study used poly(lactic-co-glycolic acid) (PLGA) as the printing resin and extrusion-based 3D printing to fabricate scaffolds. Although PLGA has been widely used as a biocompatible material in the tissue engineering field [13-15], 3D printing PLGA with direct melt method has not been well developed. Most reported attempts require solvents or binders during the fabrication process [16, 17], with significantly increased complexity of fabrication and risk of solvent residue remaining in the printed scaffolds. Therefore, we are interested in using PLGA as a model material – with no additional ingredients needed – to develop a systematic procedure for direct melt extrusion 3D printing. In addition, although the effect of PLGA composition on the degradation rate and mechanical properties have been investigated, how these material properties contribute in 3D printing quality or affect the printing conditions are not well known. We also demonstrated how material properties affect the printing outcome and evaluated the printed scaffold. Therefore, this study would be a suitable guide for researchers want to 3D print PLGA for a particular application, but not sure which type and what quality they could obtain. In this study, five different types of PLGA with various molecular weights, lactic acid (LA):glycolic acid (GA) ratios, and end caps were chosen to investigate the dependence of the extrusion process on the polymer composition. In the process of 3D printing thermoplastic material, it is essential to understand how material properties and printing parameters (such as temperature and pressure) correlate with each other. Therefore, our first objective was to determine the material rheology and temperature range suitable for high quality printing. Our second objective was to use a statistical model to investigate how printing parameters, polymer composition, and scaffold fiber orientation correlate with each other and affect the 3D printing quality. Overall, we demonstrated success of printing scaffolds with precise structures, and quantitatively evaluated the material and printing parameters effects on printing quality when using different needle sizes. We also investigated the effect of PLGA compositions on the scaffold degradation, mechanical and water adsorption properties.

Materials and Methods

Materials

PLGA with different compositions (LA:GA ratio, molecular weight, and end cap) was purchased from Lactel (Birmingham, AL) (PLGA 0.5-10kD-ester) and PolySciTech (West Lafayette, IN) (other four compositions). We selected five different types of PLGA to systematically investigate the impact of material composition on the quality of 3D printed scaffolds. **Table 1** details the five material compositions and assigns a code to each composition.

Table 1. Summary of different PLGA compositions. Different types of PLGA were investigated in this study, and we refer to their composition code in the figures and manuscript. For the composition code, the first term is the lactic acid percentage, the second term is the rounded molecular weight, and the last term is the end cap type of the co-polymer.

Composition Code	Polymer	LA:GA ratio	Molecular Weight (kDa)	End Cap
0.5-10kD-ester	PLGA 1	50:50	9.73	ester
0.5-30kD-ester	PLGA 2	50:50	30.3	ester
0.6-42kD-ester	PLGA 3	60:40	42.6	ester
0.6-34kD-acid	PLGA 4	60:40	33.8	acid
0.85-62kD-ester	PLGA 5	85:15	61.9	ester

*LA:GA = lactic acid : glycolic acid

Differential Scanning Calorimetry

Modulated differential scanning calorimetry (mDSC) was performed to determine the glass transition and thermal energy at the printing temperature using TA DSC Q100 (TA Instruments, New Castle, DE) to obtain the potential printing temperature range. Five different types of unprocessed PLGA were sealed in hermetic aluminum pans (TA Instruments, New Castle, DE). Materials were quickly equilibrated at the highest temperature and kept isothermal for 5 minutes. The temperature was ramped at 10 ºC /min to -20ºC, and then a scan from -20ºC to 200ºC at a rate of 10ºC/min was conducted and recorded.

Rheology

The rheological studies were conducted on a strain-controlled RDA III rheometer (Rheometric Scientific Inc. Piscataway, NJ). All experiments were conducted using 25 mm flat plate geometry. Samples were maintained at the safe temperature according to the DSC results in closed oven. Each temperature was given a soak time / equilibration time of 15 min before experiments were conducted. Strain sweep was first performed to identify the linear viscoelastic region (LVR). Subsequent tests were performed at 10% strain within the LVR. Frequency sweep (0.1 rad/sec - 100 rad/sec) was performed at each temperature starting from 80^{O}C at 10^{O}C increments. Frequency sweep was performed instead of strain-rate sweep to make sure the sample was in LVR. Strain sweep was also performed (0.1/sec – 100/sec) for comparison. Data was recorded and analyzed using TA orchestrator software (TA Instruments, New Castle, DE).

Gel Permeation Chromatography

The molecular weight of the unprocessed PLGA and printed PLGA was determined by gel permeation chromatography (GPC) using a Waters Alliance Separations Module e2695, Waters 2414 Refractive

Index Detector, and Waters HSPgel columns in series (HR MB-L and HR 3.0 columns, 6.0 mm ID × 15 cm) (Waters, Milford, MA) [18]. For printed PLGA, scaffold was fabricated using conditions summarized in **Table 2**, then a small piece of the printed scaffold was cut and dissolved in tetrahydrofuran for the test. Polystyrene standards were used to report the relative molecular weights. The standard curve was generated from a 10-point calibration using Agilent EasiCal polystyrene standards. The data analysis was performed using Waters Empower 3 Chromatography Data software. Three samples of each composition were performed for statistical analysis.

Scaffold Printing

3D square models with a dimension of 4 mm (length) × 4 mm (width) × 1.5 mm (height) were designed in SolidWorks (Waltham, MA). According to the manufacturer's (EnvisionTEC, Gladbeck Germany) instruction, the model scaffold was sliced into layers with a slicing thickness equal to 80% of the needle inner diameter (ID) before printing. For 0.2 mm and 0.4mm ID stainless steel needles, we used 0.16 mm and 0.32 mm slicing thicknesses, respectively (Bioplotter RP, EnvisionTEC). Scaffolds were printed under various conditions including: needle size, temperature, pressure, printing speed, fiber spacing, and inner fiber pattern. The scaffolds were printed on double sided tape for better adhesion. The platform temperature was kept at 15 ^{O}C. Three patterns were fabricated for the quality assessment (1. Parallel strands with 0.2 mm fiber spacing, 2. 0º/90º crosshatch where the printed layers are alternatively perpendicular to each other with 0.2 mm fiber spacing. 3. 45º/45º crosshatch with 0.4 mm fiber spacing). Each combination with different printing parameters for different types of PLGA was printed for further evaluation and statistical analysis. For degradation and mechanical testing, 0°/90° crosshatch pattern was used to test the scaffold properties.

Micro-Computed Tomography

Micro-computed tomography (microCT) was used to noninvasively image and characterize the printing quality of the scaffolds. Scanning was performed on a microCT 100 (SCANCO Medical, Brüttisellen, Switzerland) operated at 55 kVp (peak kilovoltage), 9 mm voxels, and 200 mA. The resulting 3D datasets were segmented using thresholds (lower: 60, maximum: 1000), with gauss sigma (0.8) and support (1) values to separate 3D printed pores and pores within the polymer [19]. We used a peak histogram approach to determine the threshold segmentation values so that the 3D scaffold can be identified from the background visually. The 3D images were evaluated for fiber diameter, fiber spacing, and porosity using Scanco's Image Processing Language (IPL). After processing, each fiber diameter of the whole scaffold was automatically calculated. These numbers were used to report the average yield fiber diameter of scaffold printed with different PLGA and various printing conditions.

Scanning Electron Microscopy (SEM)

The PLGA scaffold sample for SEM was sputtered coated with gold and imaged using Schottky field emission gun scanning electron microscope (Hitachi SU-70 FEG SEM, Hitachi High-Technologies, Germany). The sample was imaged under vacuum with 2kV voltage. The magnification was 30 times.

Statistical Analysis

For GPC results, data were analyzed using Student's t test. A significant level of 95% was chosen, and a *p*-value less than 0.05 was considered to indicate a significant difference between samples.

Statistical models were utilized to: (1) evaluate the effects of different experimental factors, including LA:GA ratio, end cap, molecular weight, temperature, pressure, speed, and fiber pattern, on the error of 3D printing (ε), defined as

$$\varepsilon = \frac{|d_{fiber} - d_{needle}|}{\mathrm{d}_{needle}} \times 100\% \qquad \textbf{Equation 1}$$

where d_{fiber} is fiber diameter and d_{needle} is needle diameter; (2) build a model to predict the error/accuracy of 3D printing under given experimental conditions (i.e. material composition and printing conditions, listed in Figure 3a). The experimental data were separated into two groups based on d_{needle} (0.2 mm or 0.4 mm). For the group with d_{needle} = 0.4 mm, all experimental factors were used in the linear model. Pressure was excluded in d_{needle} = 0.2 mm group since the values were kept constant for all experimental groups (9 bars). A linear regression was performed using statistical package R. The *p*-values of β coefficients in the linear models were used to determine if the experimental factors significantly impacted ε. An experimental factor was considered significant if its *p*-value < 0.05. To evaluate the predictive performance of these linear models, root mean squared error (RMSE) was used to compare the predictions from the linear regression model ($\hat{\varepsilon}_i$, predicted error) and the actual 3D printing error (ε_i), for a sample size, *n*.

$$RMSE = \sqrt{\frac{\sum_{i=1}^{n} (\hat{\varepsilon}_i - \varepsilon_i)^2}{n}} \qquad \textbf{Equation 2}$$

In Vitro Degradation

Scaffolds printed with a 0º/90ºcrosshatch pattern (0.2 mm fiber spacing) were chosen as an example in the following scaffold characterization tests. The scaffolds were placed in 5ml of PBS (Sigma-Aldrich, St. Louis, MO) and shaken at 37ºC at 65 rpm for *in vitro* degradation. The original weight of each scaffold was recorded. The pH of each sample was measured and PBS was changed every 7 days to make sure it

was maintained at 7.4. Before measuring the wet weight, the scaffolds were removed from the PBS and then dried with a paper towel. After measuring wet weight, the scaffolds were lyophilized to determine the dry weight [20]. To measure the wet scaffold mass, scaffolds were removed from PBS, dried with a paper towel, and then the weight was measured. For water adsorption statistical analysis, percentage water uptake was compared between each two groups.

Compression Mechanical Testing

Compression mechanical testing was performed on degraded scaffolds using an Instron mechanical testing system (33R/4465) (Norwood, MA). At each time point, fully hydrated scaffolds were removed from PBS and immediately tested in air (days 7, 14, and 21). Five scaffolds of each PLGA composition from each time point were tested (0º/90º crosshatch pattern was chosen as a standard pattern for testing). The compressive mechanical properties during degradation were evaluated. Samples that lost the shape due to significant degradation were excluded from the measurement and indicated by "-" in **Figure 4b**. A 50N load cell was applied to all samples. Samples were compressed at a displacement rate of 0.5 mm/min and values were recorded every 10 ms. A pre-load of 0.05N was applied to all samples reduce the noise of the measurement. The compression was maintained until a drop of at least 10% in force was observed or it reached the machine protection distance. Engineering stress and strain were calculated based on original cross-sectional area and height of the wet scaffolds measured before testing. For each time point, compressive stress and strain was recorded. Compressive modulus was calculated using R software to determine the linear region and the slope of the stress-strain curve. The program found the linear region (which determines the compressive modulus based on definition) that contained more than 100 data points and searched for the longest valid region for the calculation, which has $R^2 \geq 0.95$. The slope of the region is the calculated as compressive modulus.

Results

It is important to understand the basic material behavior before 3D printing. In particular, when using a high temperature extrusion technique, it is essential to quantify the thermal response of the material. First of all, we studied the heat flow of the five types of PLGA when temperature changes **(Figure 1a)**. Based on the plot, we observed a glass transition temperature around 35°C to 60°C. By comparing the glass transition temperature for the various material compositions, it was indicated that the glass transition temperature largely depends on the molecular weight. PLGA 0.5-10kD-ester with a low molecular weight has a dramatic lower temperature compared to other PLGA. Although each composition had a different LA:GA ratio and end cap, the glass transition starting points were similar among groups with comparable

molecular weights. The PLGA 0.85-62kD-ester group (with the highest LA:GA ratio and molecular weight) exhibited the highest glass transition temperature around 57°C. The energy of the materials was stable without a significant energy wave in the temperature range that includes the printing temperature, which demonstrates that the high temperature printing conditions do not break down the polymer.

The rheology plot was presented as viscosity versus temperature for all five PLGA compositions **(Figure 1c)**. The temperature range includes all extrusion temperatures. Viscosity decreased linearly with increasing temperature for all samples. At a given temperature, for ester end capped-PLGA groups, the viscosity was higher for compositions with higher LA:GA ratios and/or higher molecular weights. In particular, the acid end cap-PLGA group showed a significantly lower viscosity compared to the ester end cap-PLGA groups. The viscosity at the optimized printing temperature for each group also depended on the selected needle size. For effective extrusion, the viscosity of the polymer was observed in the range of 0.1-10 Pa•s.

Gel permeation chromatography was performed to compare the molecular weight of different types of PLGA before and after printing. In general, other than the PLGA 0.85-62kD-ester group, the molecular weight of printed PLGA and the unprocessed PLGA were significantly different **(Figure 1a)**. By comparing 0.5-10kD-ester and 0.5-30kD-ester, the PLGA with lower molecular weight has a relatively lower percentage molecular weight loss. We observed that the ester end cap is more resistant to the temperature increase, which is consistent with the results observed in rheology. Notably, in the rheology test, the ester end cap PLGA also showed greater resistance to high temperature. As the LA:GA ratio increases from 50:50 to 85:15, the molecular weight loss is inversely related to the increased LA ratio.

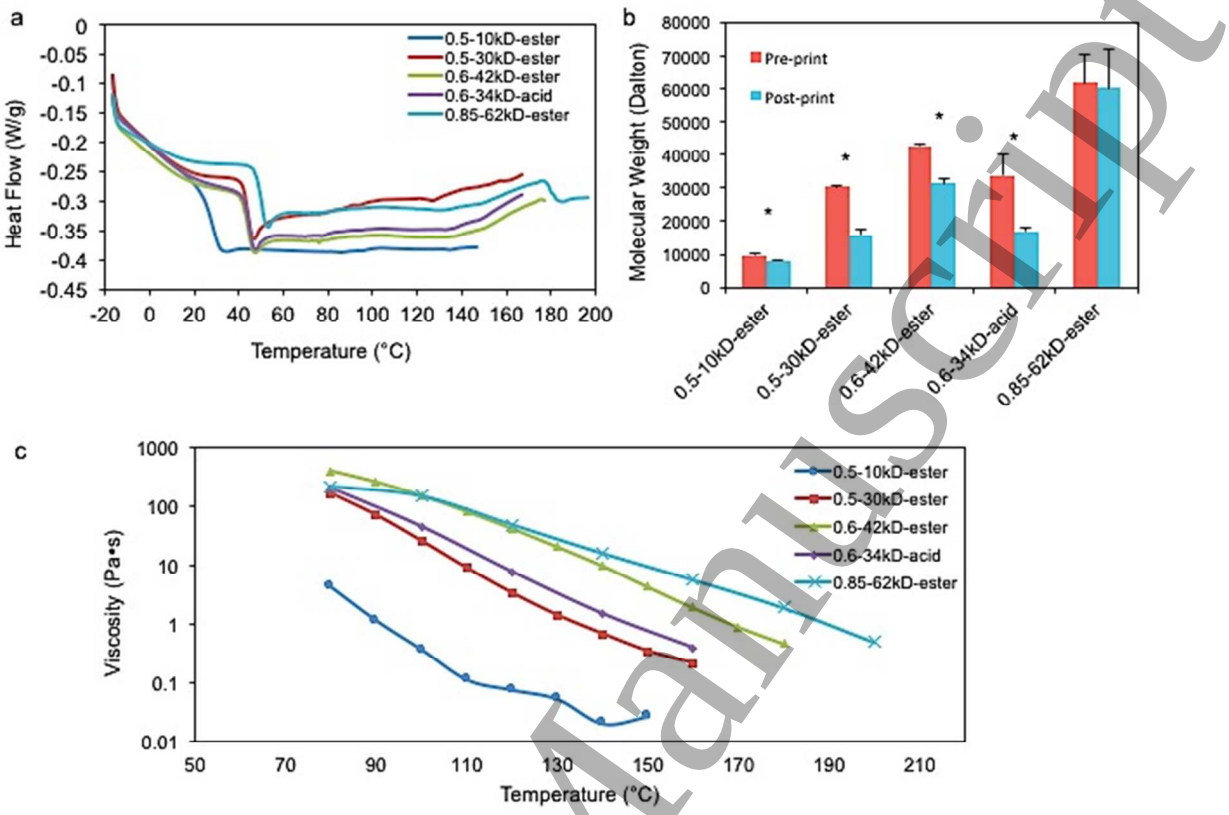

Figure 1. Evaluation of PLGA Material Properties Before and After 3D Printing. a. Differential scanning calorimetry assay showed normalized heat flow as temperature increases. PLGA glass transition was observed between 35°C to 60°C, which is significantly lower than extrusion temperature. **b.** Comparison of molecular weight of five PLGA compositions before and after printing. * indicated significant difference in each group (p-value < 0.5). **c.** Complex viscosity of different types of PLGA as a function of temperature. Viscosity generally decreased with increasing temperature. The complex viscosity was measured at a fixed frequency of 10 rad/s.

Scaffolds with designed patterns were successfully fabricated using direct melt extrusion **(Figure 2)**. Based on the designed dimension, scaffolds with 9 layers were built layer-by-layer, and the printer camera took images of single printed layers. The programmed spacing of the adjacent fibers for the parallel and crosshatch patterns is 0.2 mm. The programmed spacing of the adjacent fibers for 45° crosshatch pattern is 0.4 mm. (In Figure 3, "pattern" is simplified to the spacing between adjacent fibers in mm to transfer this categorical factor to numerical factor). The printed scaffolds had a comparable pattern to the CAD model for each layer. MicroCT was performed to reveal the details of the complete 3D printed scaffolds. This non-destructive technique can further quantify the scaffold structural properties, such as fiber diameter, which was used as a metric to assess printing quality.

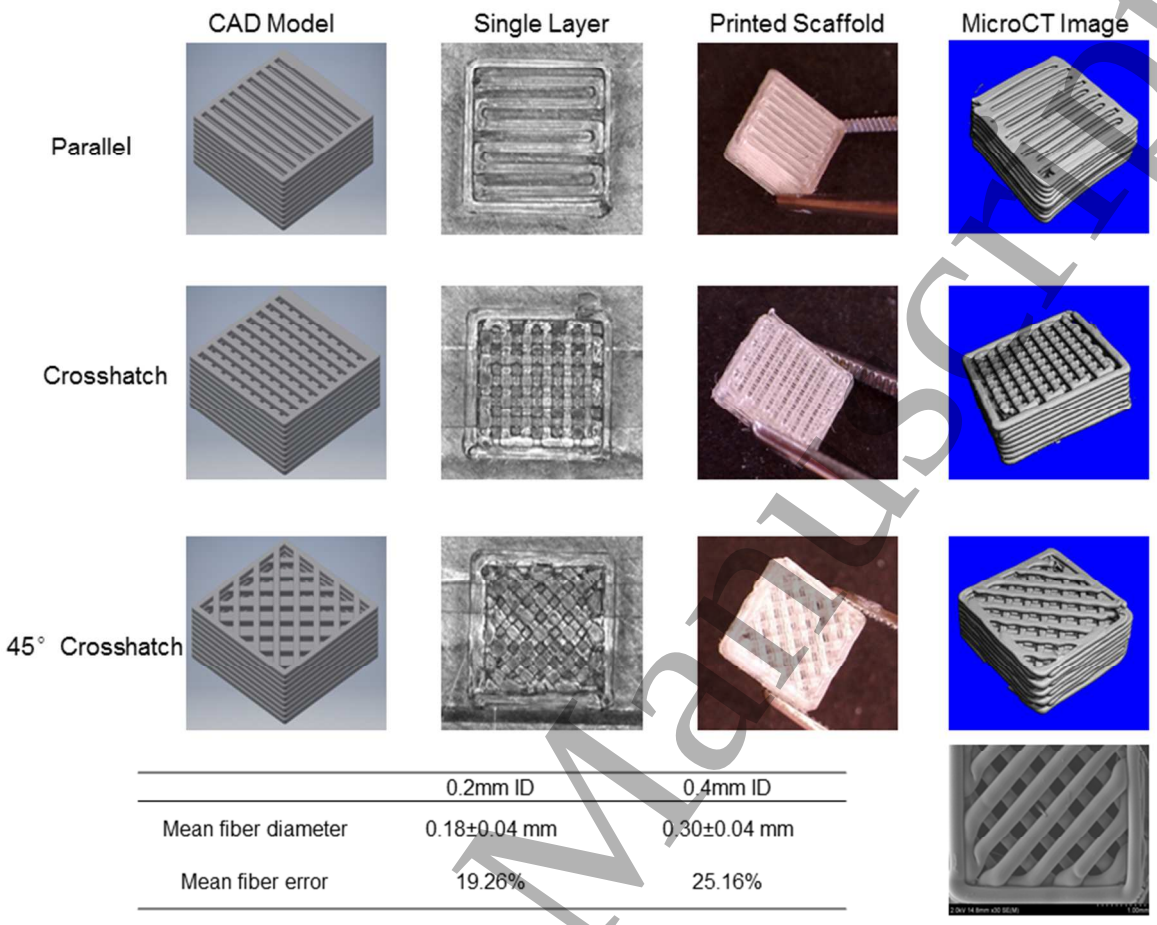

	0.2mm ID	0.4mm ID
Mean fiber diameter	0.18±0.04 mm	0.30±0.04 mm
Mean fiber error	19.26%	25.16%

Figure 2. Scaffold Design and Image Analysis. 3D printed PLGA scaffolds with distinct patterns (from top to bottom: parallel, 0°/90° crosshatch*, and 45°/45° crosshatch) were printed in a dimension of 4 mm × 4mm ×1.5 mm. From left to right column: the CAD model design, a single layer picture recorded by the printer camera, a 3D view of printed 9-layer scaffold, and a microCT-reconstructed image are shown. The table summarizes the average fiber diameter and printing accuracy (mean fiber error) of printed scaffolds using different needle sizes. A smaller needle size resulted in higher printing resolution with a smaller error. *Crosshatch means that the printed layers are alternatively perpendicular to each other (in a 0°/90° or a 45°/45° alternating pattern, where the angle is measured between inner structure and outer contour). SEM image of the printed scaffold showed smooth surface and clean fibers.

The printing conditions to form fine fibers that will yield the programmed fiber diameter (±0.01 mm) are listed in **Table 2**. Notably, since the three main printing parameters are not independent of each other, other combinations, such as higher temperature with higher speed, can also be applied to achieve similar printing quality. However, in order to minimize the degradation that could be caused by extreme temperature, the conditions summarized in **Table 2** were set at a lower temperature with a reasonable printing speed. As the needle inner diameter is reduced by half, the required temperature and pressure for extrusion increased significantly. For the 0.2mm ID needle, the pressure was kept at 9 bars, which is the safe upper limit our printer could provide. Comparing PLGA with different compositions, the temperature

required for extrusion depends strongly on the molecular weight, although LA:GA ratio and end cap also play a role in determining the printing conditions. In general, higher molecular weight, higher LA:GA ratio, and an ester cap demand more extreme processing temperatures and pressures.

Table 2. Printing conditions for PLGA with different compositions. Printing conditions such as temperature, pressure, and speed were optimized to print fine fibers for each composition.

Composition Code	0.2 mm ID*			0.4 mm ID		
	Temperature (°C)	Pressure (bar)	Speed (mm/s)	Temperature (°C)	Pressure (bar)	Speed (mm/s)
0.5-10kD-ester	110	9	1.5	95	7.5	1.5
0.5-30kD-ester	135	9	0.7	125	8	1.5
0.6-42kD-ester	165	9	0.7	140	9	0.5
0.6-34kD-acid	150	9	1.5	130	8	1
0.85-62kD-ester	170	9	0.5	145	8	0.5

* Two syringe needles were used to print PLGA fibers, ID = inner diameter

In order to understand how material properties and printing parameters determine the extrusion fabrication accuracy, PLGA compositions with different LA:GA ratios, molecular weights, and end caps were printed at various temperatures, pressures, speeds, and patterns. Each combination was printed and then imaged and analyzed using microCT and the supporting software. From the 3D reconstruction results, the fiber diameter as a function of different printing parameters is listed in **Figure 3a.**

We evaluated the printing accuracy based on different extrusion needle sizes **(Figure 2)**. The printing error (or fiber error) was calculated from **Equation 1**. The statistical results summarized from different types of PLGA gave an average fiber diameter of 0.1773 mm when using a 0.2mm ID needle and an average fiber diameter of 0.2993 mm when using 0.4 mm ID needle. The calculated error when using 0.2 mm ID is lower than the 0.4 mm ID. These interesting findings indicate that a smaller needle size requires more extreme processing conditions (i.e. higher temperature and pressure) but also produces more precise fibers since the conditions are more restricted and more close the optimized case.

A linear regression model was applied to the experimental data to determine the impact of each material and printing parameter on the printing accuracy **(Figure 3b)**. In the results, factors with a *p*-value less than 0.05 were considered as significantly impactful on the printing error (**Equation 1)**. Since the same pressure was applied during fabrication using the 0.2 mm ID needle, this factor was not considered in the 0.2 mm statistical model. With the 0.2 mm needle size, the material parameters including LA:GA ratio

(ratio), molecular weight (Mw), and end cap, and printing parameters, such as temperature, speed, and pattern (simplified as the fiber spacing for the parallel, 0º/90º crosshatch, and 45º/45º crosshatch patterns) , all played a significant role in determining the precision of printing. The small p-value associated with the material parameters indicated them as significant factors for the 0.2 mm needle. However, when using a larger needle with 0.4 mm ID, we observed that the printing accuracy relies more on the printing parameters, and some printing parameters became less significant. In both groups, the designed pattern did not have a significant impact on the printing accuracy, indicating the feasibility of using this technique for broader applications containing complex structures.

0.2 mm Needle Linear Regression

$$Error = 2.79 - 3.54 \times \text{ratio} + 6.561 \times 10^{-5} \times \text{Mw} - 0.326 \times \text{endcap} - 0.00217 \times \text{temperature} + 0.5539 \times \text{speed} - 0.0555 \times \text{pattern}$$

Equation 3

0.4 mm Needle Linear Regression

$$Error = 0.6648 + 0.0846 \times \text{ratio} - 1.36 \times 10^{-5} \times \text{Mw} - 0.3756 \times \text{endcap} + 0.013 \times \text{temp} - 0.1555 \times \text{pressure} - 0.2947 \times \text{speed} - 0.0237 \times \text{pattern}$$

Equation 4

The linear models showed an R^2 of 0.76 for the group with d_{needle} = 0.2 mm and 0.74 for the group with d_{needle} = 0.4 mm. Both groups exhibited significant linear relationships between the experimental conditions and the resolution of 3D printing (p-value = 3.21×10^{-4} for the 0.02 group and 1.81×10^{-4} for the 0.04 group)(for linear model in Figure 3b). The RMSEs are 5.52×10^{-3} and 3.75×10^{-3} for the 0.2 mm and 0.4 mm group respectively, suggesting that our linear models performed well in prediction in both scenarios.

a

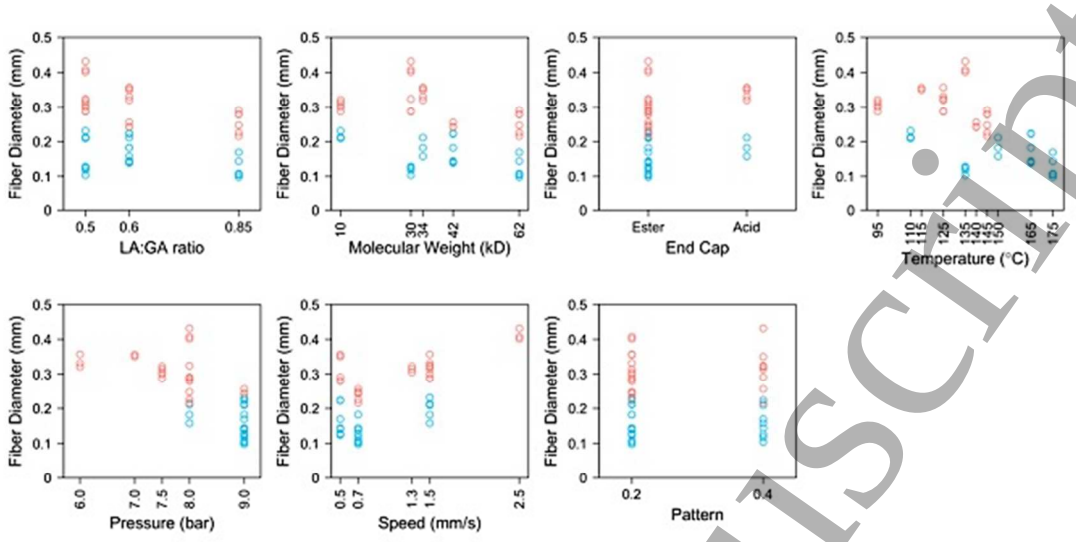

b

	0.2 mm ID			0.4 mm ID	
	Interaction coefficient	p-value		Interaction coefficient	p-value
LA/GA ratio	Significant	0.0017	LA/GA ratio	Not significant	0.91
Molecular weight	Significant	0.00019	Molecular weight	Not significant	0.22
Endcap	Significant	0.028	Endcap	Significant	0.010
Pressure	N/A	N/A	Pressure	Significant	0.048
Temperature	Significant	0.000068	Temperature	Significant	0.025
Speed	Significant	0.022	Speed	Significant	0.0025
Pattern	Not significant	0.78	Pattern	Not significant	0.88

c

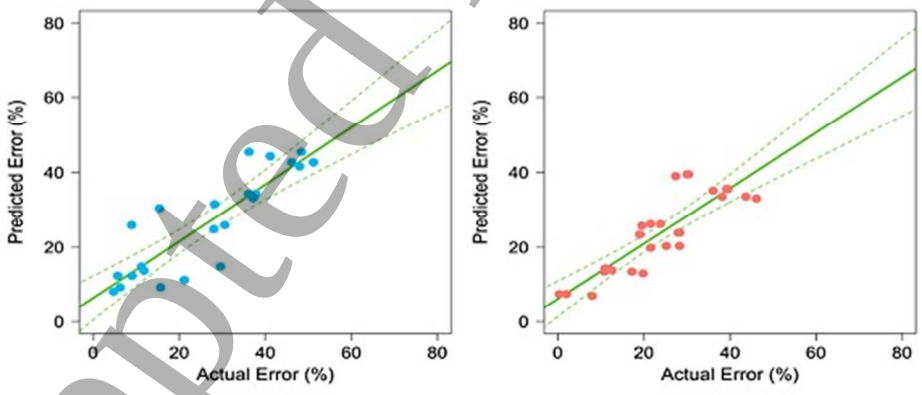

Figure 3. Statistical Analysis of Printing Resolution. a. Fiber Diameter Distribution with Different Material Properties and Printing Parameters. Data points associated with 0.2 mm ID needle were shown in blue, while data points associated with 0.4 mm ID needle were shown in red. X-axis includes material and printing control parameters, and y-axis shows measured fiber diameter calculated from microCT scanning. **b.** Main effect analysis of the material parameters and printing parameters impact on printing accuracy. Two significant digits were applied in p-value analysis. A p-value < 0.05 is considered to be

statistically significant. **c.** Evaluation of the Accuracy of the Predicted Model. Linear regression of predicted error using equation 5 & 6 and actual error calculated from microCT evaluation (Left: 0.2 mm ID needle, Right: 0.4mm ID needle). Both models showed strong linear relationship between the predicted error and actual error, indicating a precise prediction potential of our model.

We further investigated if our predicted values using **Equation 3** and **Equation 4** were capable of representing the actual error **(Figure 3c)**. Linear regression was performed to evaluate the relationship between the actual errors and the errors predicted from the linear models.

0.2 mm Needle Linear Regression Error

$$\text{Predicted Error} = 0.75855 \times \text{Actual Error} + 0.06384 \qquad \textbf{Equation 5}$$

$p\text{-value} = 6.45 \times 10^{-8}$

0.4 mm Needle Linear Regression Error

$$\text{Predicted Error} = 0.73987 \times \text{Actual Error} + 0.06151 \qquad \textbf{Equation 6}$$

$p\text{-value} = 8.88 \times 10^{-9}$

Both cases suggest that there is a significant linear relationship between the actual errors and the predicted errors because the p-value is much less than 0.05. Based on statistical precision of our model, we believe this model could provide a good prediction of printing outcome.

In order to use the printed PLGA scaffold for osteochondral defect repair, the scaffold properties were also investigated **(Figure 4)**. The scaffolds were kept on shaker at 37°C for *in vitro* degradation and the scaffold morphology and mechanical properties were evaluated. As expected, PLGA with a 50:50 LA:GA ratio experienced fast degradation with significant mechanical strength loss over 21 days [21]. Both 50:50 groups lost about 50-60% mass during the 21-day incubation **(Figure 4a)**. In particular, the acid end cap played a significant role in accelerating the degradation and resulted in weaker compressive modulus. The acid end capped PLGA scaffolds lost around 80% mass after 21 days at 37 °C. The compressive modulus of PLGA 0.5-10kD-ester was not measurable due to the structural loss during its rapid degradation. With a 85:15 LA:GA ratio and moderate molecular weight, PLGA 0.85-62kD-ester showed a steady degradation during early time points **(Figure 4b)**. In the water adsorption test, the wet mass at each time point was compared with the initial scaffold mass **(Figure 4c)**. The printed scaffolds with different polymer composition all demonstrated the ability to adsorb water. In general, PLGA with a lower LA:GA ratio and an acid end cap was able to uptake water more readily during *in vitro* incubation. Based on the

statistical analysis comparing significance between each two groups, by day 7, the acid end capped PLGA adsorbed significantly more water than the ester end capped PLGA.

a

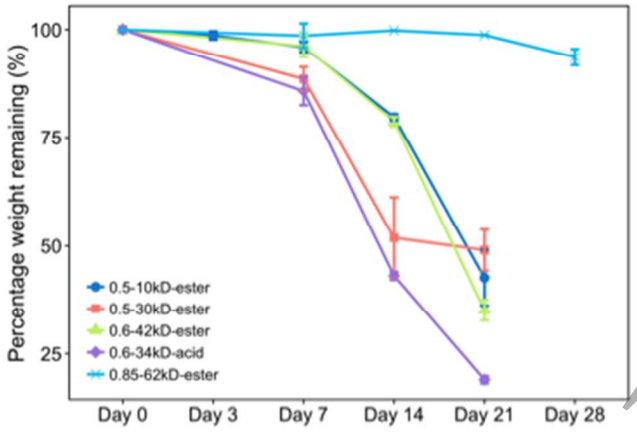

b

	0.5-10kD-ester	0.5-30kD-ester	0.6-42kD-ester	0.85-62kD-ester
Day 7	0.0015±0.0005MPa	0.34±0.1MPa	0.017±0.008MPa	1.79±0.8MPa
Day 14	-	0.0019±0.0004MPa	0.0033±0.0002MPa	4.44±1.8MPa
Day 21	-	-	-	1.72±0.3MPa
Day 28	-	-	-	1.82±0.7MPa

c

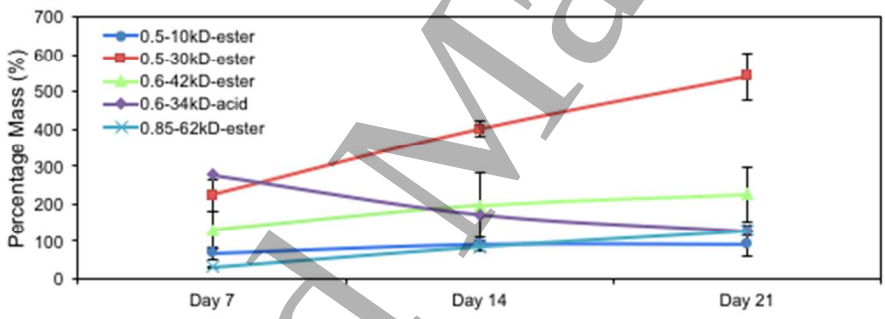

Figure 4. **Printed scaffold properties. a.** Degradation profile of scaffolds printed with different types PLGA. The mass remaining of different types of PLGA was recorded. PLGA with lower molecular weight and acid end cap experienced faster degradation. **b.** Compressive modulus of scaffolds with different compositions during *in vitro* degradation. PLGA with moderate molecular weight and an ester end cap showed stable compressive mechanical properties during the study. **c.** Water adsorption of the printed scaffold. The printed scaffolds showed ability to uptake water. Scaffolds printed with an acid end and more PGA content adsorbed more water during the course of study because the material is more hydrophilic.

Discussion

In this study, we evaluated the feasibility and impact factors of using a direct melt extrusion printing method to process PLGA, a thermoplastic material. At first, mDSC was performed to determine the glass transition and thermal energy at the printing temperature. The stable thermal energy at our desired printing temperature confirms that the high temperature processing is not likely to break down the

material. Therefore, DSC may serve as an initial step to consider the processing temperature for new material printing. In order to prevent breakdown of the material, the printing temperature should be kept at a range higher than the glass transition temperature but lower than the thermal molecular decomposition temperature. Particularly in extrusion printing, rheology is an important factor to evaluate, which can be utilized as a further guide to determine the fabricating conditions [22]. The rheological properties of five types of PLGA were analyzed. In this case, the plot of complex viscosity at certain frequency equals to the viscosity at certain shear rate according to Cox-Merz rule. To protect the material under shear, the experiment was conducted under oscillatory setting so the complex viscosity was measured. We observed effective extrusion and an optimal printing resolution when the viscosity was within the range of 0.1-10 Pa•s, which is consistent with documented ranges using other materials [12, 23, 24]. Specific viscosity at certain extrusion condition depends on the needle size, where smaller needle requires lower viscosity for effective extrusion. The linear relationship between viscosity and temperature confirmed that a high temperature extrusion technique would not harm to the polymer structure during printing. However, the GPC data comparing the molecular weight between unprocessed PLGA and printed PLGA revealed a molecular difference. This could be a result from the lower printing temperature since the melting temperature mostly relies on the molecular weight. This indicates that for actual applications, we may take account the molecular weight change after printing if it is a critical factor to consider in the further studies. These results indicate that although the direct melt extrusion procedure does not seem to drastically alter the polymer structure, the printed scaffolds may still have different mechanical and degradation properties as casted scaffolds, which should be considered in the future applications.

We performed a linear regression model to systematically investigate the effects of material composition and printing parameters on printing accuracy. In general, we found that using a smaller needle results in a smaller error. The printing conditions are unlikely to have a linear relationship with the viscosity or the resulted printing error. An exponential relationship between the temperature and viscosity would be one reason that when using smaller diameter needle, the fiber diameter change is more resistant to the printing condition parameters change. The Hagen-Poiseuille Law **(Equation 7)** [25] provides the connection between the viscosity, needle size and volume of plotting material. Due to a proportional fourth power in needle size in the equation, the needle diameter affects the dispensed material at a given time dramatically, which makes the fineness of extruded fiber harder to control. An interesting finding we learned from the main effect analysis of the control parameters and fiber accuracy is that the printing error is more material-dependent when using a small diameter needle while more printing condition dependent when using a larger diameter needle.

By comparing the significant factors between printing using small needle and large needle, we observed that when using smaller diameter needle, the material properties play a more important role in the resulting printing quality. In contrast, when using a large diameter needle, the printing parameters such as pressure, and speed became more significant to determine the fiber quality. One explanation could be that when the needle diameter is very small, the printing conditions are strict and extreme without much flexibility. As a result, the printing outcome most depends on the material itself. However, when the needle diameter increases, multiple 1st order factors in the Hagen-Poiseuille Law can be considered as predominant factors to compensate the material property difference.

$$V = \frac{\pi \times \Delta p \times \Delta t}{8 \times \eta \times L} \times r^4 \qquad \textbf{Equation 7}$$

where V is the volume of the plotting material, η is the dynamic viscosity, p is pressure, t is dispensing time, L is needle length and r is the needle diameter.

In the statistical analysis, the small RMSEs values, 5.52×10^{-3} and 3.75×10^{-3} for the 0.2 mm and 0.4 mm group, respectively, suggest that our linear models **(Equation 3 and 4)** performed well in the prediction of yield printing accuracy. We also demonstrated that our prediction model has a strong linear relationship relating to the actual accuracy, which further confirmed the power of this established prediction model. However, statistically, a new set of experimental data with new input material and printing parameters is needed to test the true power of our model in future applications and analysis.

In terms of printed scaffold properties, from the mechanical properties of the scaffolds during degradation, PLGA scaffolds with a low LG:GA ratio quickly lost their compressive strength and morphology in the first two weeks. In addition, an ester end cap is beneficial to stabilize the material during both the printing process and degradation. Since glycolic acid is more hydrophilic than lactic acid due to the presence of methyl side groups in LA, scaffolds with a lower LA:GA ratio were more capable of adsorbing water [26]. An acid end cap also decreases the hydrophobicity, in addition to accelerating the degradation. Therefore, for 3D printed scaffolds, PLGA that has a high LA:GA ratio and ester end cap may serve as a suitable scaffold for cartilage regeneration, considering the relatively slow degradation rate and similar compressive mechanical strength to native human cartilage [27]. For future applications, a wide variety of PLGA compositions can be combined with direct melt extrusion to design 3D printed implants requiring unique chemical, mechanical, and degradation properties.

Conclusions

In conclusion, for the applications of 3D printing thermoplastic material using direct melt extrusion, it is important to first understand the material properties and use the analysis as a guide to determine optimal printing conditions. For applications that prefer to maintain scaffold structure and mechanical strength over a relatively long period, it is recommended that a high LA:GA ratio is chosen for the printing process. PLGA with an ester end cap also demonstrated a better structural stability in 3D printing for tissue engineering applications. These well-characterized PLGA scaffolds with high resolution can be used in many tissue engineering applications. Although the techniques and discovery in this study are not restricted to a specific type of tissue or certain applications, our research mainly focuses on optimizing printing procedures and scaffold characteristics to repair osteochondral defects. This systematic study will contribute to developing standards for the 3D fabrication procedures in tissue engineering and regenerative medicine.

Acknowledgement

The authors would like to thank Dr. Josephine Lembong from University of Maryland for reviewing the manuscript and Dr. Maureen Dreher from Food and Drug Administration for microCT training. We also thank Dr. Jesse Placone for his help on 3D fabrication. This work was supported by National Science Foundation grant CBET 1264517 and CBET 1604742.

Disclosure Statement

No competing financial interests exist.

References

1. Langer R. and Vacanti J.P., *Tissue engineering.* Science, 1993. **260**(5110): p. 920-6.
2. Hollister S.J., *Porous scaffold design for tissue engineering.* Nature materials, 2005. **4**(7): p. 518-24.
3. Lee K.Y. and Mooney D.J., *Hydrogels for tissue engineering.* Chemical reviews, 2001. **101**(7): p. 1869-79.
4. Seda Tigli R., Ghosh S., Laha M.M., Shevde N.K., Daheron L., Gimble J., Gumusderelioglu M., and Kaplan D.L., *Comparative chondrogenesis of human cell sources in 3D scaffolds.* Journal of tissue engineering and regenerative medicine, 2009. **3**(5): p. 348-60.
5. Li W.J., Tuli R., Okafor C., Derfoul A., Danielson K.G., Hall D.J., and Tuan R.S., *A three-dimensional nanofibrous scaffold for cartilage tissue engineering using human mesenchymal stem cells.* Biomaterials, 2005. **26**(6): p. 599-609.
6. Hsu S.H., Yen H.J., Tseng C.S., Cheng C.S., and Tsai C.L., *Evaluation of the growth of chondrocytes and osteoblasts seeded into precision scaffolds fabricated by fused deposition manufacturing.* Journal of biomedical materials research. Part B, Applied biomaterials, 2007. **80**(2): p. 519-27.
7. Landers R., Hubner U., Schmelzeisen R., and Mulhaupt R., *Rapid prototyping of scaffolds derived from thermoreversible hydrogels and tailored for applications in tissue engineering.* Biomaterials, 2002. **23**(23): p. 4437-47.
8. Fedorovich N.E., Swennen I., Girones J., Moroni L., van Blitterswijk C.A., Schacht E., Alblas J., and Dhert W.J., *Evaluation of photocrosslinked Lutrol hydrogel for tissue printing applications.* Biomacromolecules, 2009. **10**(7): p. 1689-96.
9. Sun W. and Lal P., *Recent development on computer aided tissue engineering--a review.* Comput Methods Programs Biomed, 2002. **67**(2): p. 85-103.
10. Hutmacher D.W., *Scaffolds in tissue engineering bone and cartilage.* Biomaterials, 2000. **21**(24): p. 2529-43.
11. Moroni L., de Wijn J.R., and van Blitterswijk C.A., *3D fiber-deposited scaffolds for tissue engineering: influence of pores geometry and architecture on dynamic mechanical properties.* Biomaterials, 2006. **27**(7): p. 974-85.
12. Trachtenberg J.E. P.J.K., Smith B.T., Piard C.M., Santoro M., Scott D.W., Fisher J.P., and Mikos A.G., *Extrusion-Based 3D Printing of Poly(propylene fumarate) in a Full-Factorial Design.* ACS Biomater. Sci. Eng, 2016.
13. Pan Z. and Ding J., *Poly(lactide-co-glycolide) porous scaffolds for tissue engineering and regenerative medicine.* Interface Focus, 2012. **2**(3): p. 366-77.
14. Gentile P., Chiono V., Carmagnola I., and Hatton P.V., *An overview of poly(lactic-co-glycolic) acid (PLGA)-based biomaterials for bone tissue engineering.* Int J Mol Sci, 2014. **15**(3): p. 3640-59.
15. Seunarine K., Gadegaard N., Tormen M., Meredith D.O., Riehle M.O., and Wilkinson C.D., *3D polymer scaffolds for tissue engineering.* Nanomedicine (Lond), 2006. **1**(3): p. 281-96.
16. Chia H.N. and Wu B.M., *High-resolution direct 3D printed PLGA scaffolds: print and shrink.* Biofabrication, 2015. **7**(1): p. 015002.
17. Roy T.D., Simon J.L., Ricci J.L., Rekow E.D., Thompson V.P., and Parsons J.R., *Performance of degradable composite bone repair products made via three-dimensional fabrication techniques.* J Biomed Mater Res A, 2003. **66**(2): p. 283-91.
18. Behrens A.M., Lee N.G., Casey B.J., Srinivasan P., Sikorski M.J., Daristotle J.L., Sandler A.D., and Kofinas P., *Biodegradable-Polymer-Blend-Based Surgical Sealant with Body-Temperature-Mediated Adhesion.* Advanced materials, 2015. **27**(48): p. 8056-61.
19. Wang M.O., et al., *Evaluating 3D-Printed Biomaterials as Scaffolds for Vascularized Bone Tissue Engineering.* Advanced Materials, 2015. **27**(1): p. 138-144.

20. Chew S.A., Arriaga M.A., and Hinojosa V.A., *Effects of surface area to volume ratio of PLGA scaffolds with different architectures on scaffold degradation characteristics and drug release kinetics.* Journal of biomedical materials research. Part A, 2016. **104**(5): p. 1202-11.
21. Ozdil D. and Aydin H.M., *Polymers for medical and tissue engineering applications.* Journal of Chemical Technology & Biotechnology, 2014. **89**(12): p. 1793-1810.
22. Aho J., Boetker J.P., Baldursdottir S., and Rantanen J., *Rheology as a tool for evaluation of melt processability of innovative dosage forms.* Int J Pharm, 2015. **494**(2): p. 623-42.
23. Zhang F., Tuck C., Hague R., He Y.F., Saleh E., Li Y., Sturgess C., and Wildman R., *Inkjet printing of polyimide insulators for the 3D printing of dielectric materials for microelectronic applications.* Journal of Applied Polymer Science, 2016. **133**(18): p. 11.
24. Aho J., Boetker J.P., Baldursdottir S., and Rantanen J., *Rheology as a tool for evaluation of melt processability of innovative dosage forms.* International Journal of Pharmaceutics, 2015. **494**(2): p. 623-642.
25. Pfitzner J., *Poiseuille and his law.* Anaesthesia, 1976. **31**(2): p. 273-5.
26. Makadia H.K. and Siegel S.J., *Poly Lactic-co-Glycolic Acid (PLGA) as Biodegradable Controlled Drug Delivery Carrier.* Polymers (Basel), 2011. **3**(3): p. 1377-1397.
27. Cohen N.P., Foster R.J., and Mow V.C., *Composition and dynamics of articular cartilage: structure, function, and maintaining healthy state.* J Orthop Sports Phys Ther, 1998. **28**(4): p. 203-15.